GEOLOGICA CARPATHICA, OCTOBER 2014, 65, 5, 387–399 doi: 10.2478/geoca-2014-0022

Petrology and geochemistry of a peridotite body in Central-Carpathian Paleogene sediments (Sedlice, eastern Slovakia)

MATÚŠ KOPPA[1], FRIEDRICH KOLLER[2] and MARIÁN PUTIŠ[1]✉

[1]Department of Mineralogy and Petrology, Faculty of Natural Sciences, Comenius University, Mlynská dolina G, 842 15 Bratislava, Slovak Republic; ✉putis@fns.uniba.sk; koppa@fns.uniba.sk
[2]Department of Lithospheric Research, University of Vienna, Althanstrasse 14, Vienna, Austria; friedrich.koller@univie.ac.at

(Manuscript received February 12, 2014; accepted in revised form June 5, 2014)

Abstract: We studied representative samples from a peridotite body situated NE of Sedlice village within the Central-Carpathian Paleogene sediments in the Central Western Carpathians. The relationship of the peridotite to the surrounding Paleogene sediments is not clear. The fractures of the brecciated peridotite margin are healed with secondary magnesite and calcite. On the basis of the presented bulk-rock and electron microprobe data, the wt. % amounts of mineral phases were calculated. Most of calculated "modal" compositions of this peridotite corresponds to harzburgites composed of olivine (~70–80 wt. %), orthopyroxene (~17–24 wt. %), clinopyroxene (<5 wt. %) and minor spinel (<1 wt. %). Harzburgites could originate from lherzolitic protoliths due to a higher degree of partial melting. Rare lherzolites contain porphyroclastic 1–2 mm across orthopyroxene (up to 25 wt. %), clinopyroxene (~5–8 wt. %) and minor spinel (<0.75 wt. %). On the other hand, rare, olivine-rich dunites with scarce orthopyroxene porphyroclasts are associated with harzburgites. Metamorphic mineral assemblage of low-Al clinopyroxene (3), tremolite, chrysotile, andradite, Cr-spinel to chromite and magnetite, and an increase of fayalite component in part of olivine, indicate low-temperature metamorphic overprint. The Primitive Mantle normalized whole-rock REE patterns suggest a depleted mantle rock-suite. An increase in LREE and a positive Eu anomaly may be consequence of interactive metamorphic fluids during serpentinization. Similar rocks have been reported from the Meliatic Bôrka Nappe overlying the Central Western Carpathians orogenic wedge since the Late Cretaceous, and they could be a potential source of these peridotite blocks in the Paleogene sediments.

Key words: peridotite, petrology, geochemistry, Slovakia.

Introduction and brief geological background

The presence of meta-ultramafic rocks within (meta)siliciclastic sediments may open new insights on the mobility of serpentinized mantle fragments within accretionary and collision wedges and their interaction with continental crust (e.g. Brandon 2004; Scambelluri et al. 2004).

Representative samples were collected for study from a 500×300 m surface occurrence of an ultramafic body to the NE from Sedlice, which forms a smaller ridge in the Šariš Highlands marked on the map as the "Dunitová Skalka" ("dunite stone" of Cambel 1951; Hovorka et al. 1985). It is situated N of the zone of pre-Carboniferous metamorphosed complexes intruded by Variscan granitoids in the Branisko and Čierna hora Mountains, in the eastern part of the Central-Carpathian Paleogene flysch belt (Marschalko 1966; Plašienka et al. 1997), in the middle of basal sandstone and conglomerate beds. This zone belongs to the Central Western Carpathians (Plašienka et al. 1997). The relationship of the serpentinized peridotite body to the surrounding Paleogene sediments is not clear. The body may be a member of a buried Mesozoic complex covered by transgressive Paleogene sediments, or an olistolith within these sediments (Hovorka et al. 1985). The geological position is shown in Fig. 1.

The peridotite body near Sedlice was the subject of interests and studies of different aspects in the past. Cambel (1951) reported enstatite dunites based on microscopic and optical identification of rock-forming minerals. The rocks with increased Cpx content associated with Spl were classified as spinel lherzolites (Cambel 1951; Fejdi & Kolník 1988; Stankovič et al. 2007). These rocks contain a certain amount of opaque minerals, usually in paragenesis with spinel. Awaruite, millerite or pentlandite have been reported in the ultramafic rocks from Sedlice by Kantor (1955) and Rojkovič (1985). The spinel-group and ore minerals were studied by Kantor (1955), Rojkovič (1985), Rojkovič et al. (1978, 1979, 1982), Spišiak et al. (2000) and Mikuš & Spišiak (2007); serpentine-group minerals by Hovorka et al. (1980, 1985); geochemistry by Hovorka (1977); geothermometry and geobarometry by Fejdi & Kolník (1988), Radvanec (2000); exsolved pyroxenes by Stankovič et al. (2007); mesoscopic structures by Jaroš et al. (1981), and tracing the spatial distribution of the body by geophysical methods was performed by Gnojek & Kubeš (1991). Despite the previous results, evolution of the body placed within the Central Carpathian Paleogene sediments remains unclear or "exotic".

This paper reports the results of mineralogical-petrological, and geochemical study of the Sedlice ultramafic body in the Western Carpathians in the territory of eastern Slovakia based on the study of the mineral (EMPA) and whole-rock (XRF and ICP MS) chemical compositions of representative samples. The mantle and crustal evolution, and tectonic origin of these rocks is discussed.

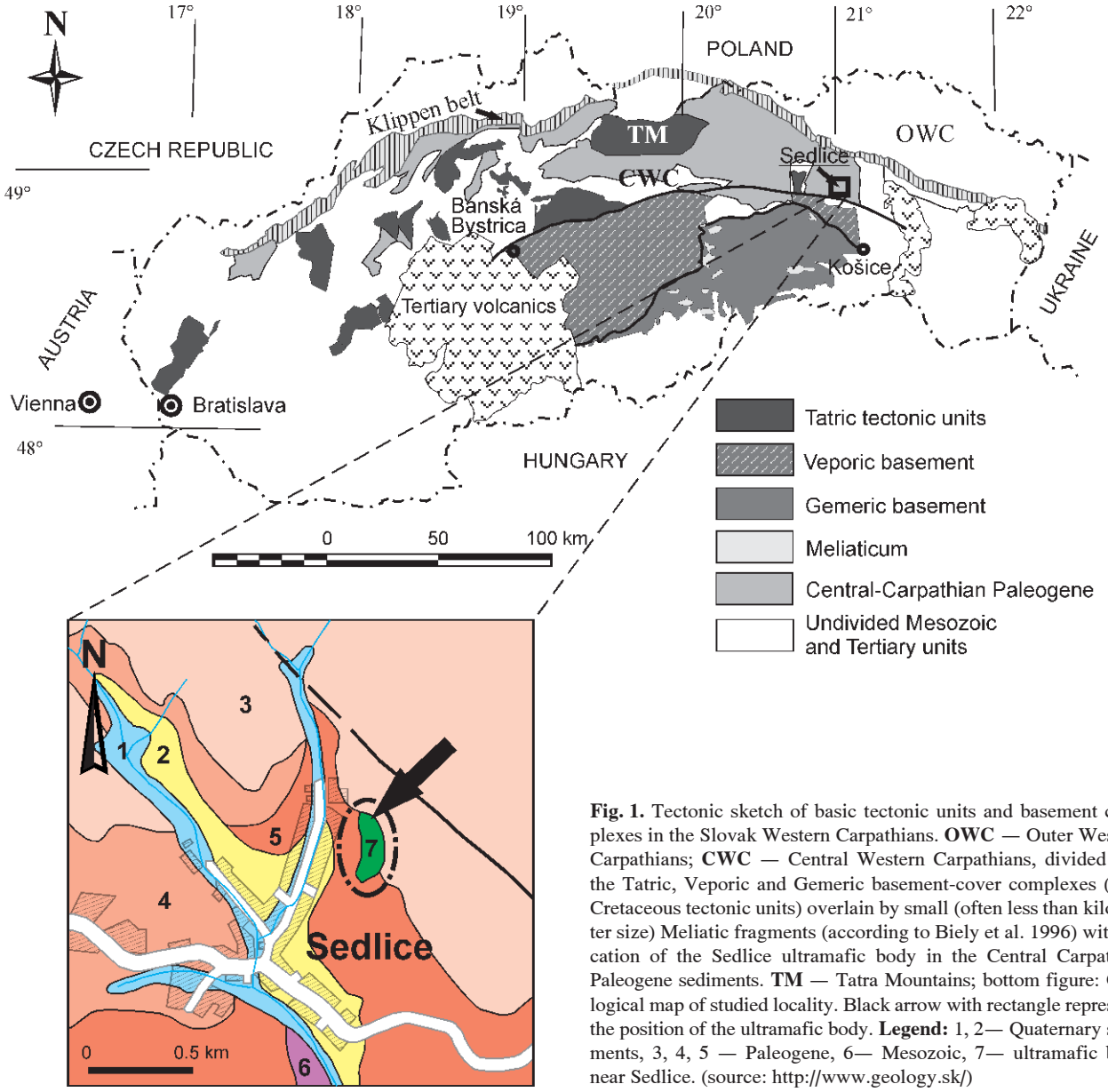

Fig. 1. Tectonic sketch of basic tectonic units and basement complexes in the Slovak Western Carpathians. **OWC** — Outer Western Carpathians; **CWC** — Central Western Carpathians, divided into the Tatric, Veporic and Gemeric basement-cover complexes (Late Cretaceous tectonic units) overlain by small (often less than kilometer size) Meliatic fragments (according to Biely et al. 1996) with location of the Sedlice ultramafic body in the Central Carpathian Paleogene sediments. **TM** — Tatra Mountains; bottom figure: Geological map of studied locality. Black arrow with rectangle represents the position of the ultramafic body. **Legend:** 1, 2— Quaternary sediments, 3, 4, 5 — Paleogene, 6— Mesozoic, 7— ultramafic body near Sedlice. (source: http://www.geology.sk/)

Materials and methods

X-ray fluorescence spectrometry was used for whole-rock major oxide and also some trace element concentrations contained in rock samples. In order to obtain representative major and trace element analyses, the rock samples were crushed in jaw mill and ground to the finest powder possible in an agate swing mill. Subsequently, the fused beads were prepared using $Li_2B_4O_7$ after the sample powders were dried at 110 °C and heated at 950–1050 °C to determine loss on drying and ignition. Major and trace element concentrations were determined on fused beads and pressed powder pellets with a wavelength dispersive X-ray fluorescence spectrometer (PHILIPS PW 2400) at the Department of Lithospheric Research, University of Vienna. The fused beads were cast using a Philips Perl X3 automatic bead machine. A rhodium anticathode was employed for the XRF analyses.

Trace element contents (including rare earth elements — REEs) were analysed by ICP-MS at the Department of General and Analytical Chemistry, Montan-University Leoben. In total 0.1 g of fine grained sample was sintered with sodium peroxide (purity 95%) to achieve complete digestion of all silicate and spinel mineral phases (Meisel et al. 2002). Measurements were performed with an Agilent 7500 ce ICP-MS with and without He collision cell mode. The International Association of Geoanalysts (IAG) Candidate reference material MUH-1, a highly depleted serpentinized harzburgite from Kraubath, Styria, Austria (Burnham et al. 2010), was used for quality control purposes. The preceding sodium peroxide sintering and acid digesting (37% HCl) followed the procedures of Meisel et al. (2002). A solution with very accurately known concentrations of Ge, In and Re (1 µl/ml) was employed as a reference material. The machine used was a standard quadrupole ICP-MS Agilent Technologies HP4500 with a v-groove

type Babington or a Burgener pumped nebulizer and a cooled quartz glass spray chamber. The whole-rock chemical compositions are reviewed in Table 1. The rock mineral compositions were calculated from the whole-rock and mineral chemical compositions (e.g. Bodinier & Godard 2007).

The chemical compositions of mineral phases were measured by Cameca SX-100 four-spectrometer electron microprobe at the State Geological Institute of Dionýz Štúr in Bratislava under the operating conditions of 15 kV accelerating voltage, 20 nA focused beam current (ϕ1–5 ηm)and 20–100 s counting time depended upon the analysed element. The standards used for calibration were: Na on albite, Si, Ca on wollastonite, K on orthoclase, Mg on forsterite, Al on Al_2O_3, Fe on fayalite, Mn on rhodonite, metallic V, Cr, and Ni, Ti on TiO_2, Sr on $SrTiO_3$, Nb on $LiNbO_3$, La on $LaPO_4$, Ce on $CePO_4$, and Ta on $LiTaO_3$. The mineral chemical compositions are reviewed in Tables 2–5.

Table 1: The whole-rock major and trace element compositions of dunite (dun), lherzolites (lherz) and harzburgites (harz) from Sedlice with mineral percentual assemblages (in wt. %). **LOI** — loss on ignition, **b.d.l.** — below detection limit, **n.m.** — not measured; Cr, Ni, Zr and Pb were measured by XRF, other trace elements by ICP-MS. * — Zr value was measured by ICP-MS.

Sample	**SE-2**	**SE-14**	**SE-15**	**SE-6b**	**SE-12**	**SE-17b**
Rock type	**dun**	**harz**	**harz**	**harz**	**lherz**	**lherz**
Ol (wt. %)	98.5	79.65	79.58	71.2	66.5	69.21
Opx (wt. %)	0	17.5	18.21	23.46	25	24.5
Cpx (wt. %)	0	2.5	1.85	4.69	8.33	5.53
Sp (wt. %)	1.5	0.35	0.36	0.65	0.17	0.76
Major elements (wt. %)						
SiO_2	38.47	39.11	41.00	41.02	42.70	40.22
TiO_2	0.04	0.05	0.05	0.06	0.06	0.07
Al_2O_3	0.13	0.48	0.43	1.31	1.74	1.69
Fe_2O_3	8.37	7.97	8.35	8.23	8.51	8.08
MnO	0.11	0.11	0.11	0.11	0.12	0.11
MgO	41.09	41.51	42.93	40.24	40.19	38.15
CaO	0.69	1.62	0.58	1.21	2.10	1.45
Na_2O	0.01	0.02	0.02	0.03	0.03	0.04
K_2O	0.02	0.01	0.02	0.02	0.02	0.02
P_2O_5	0.03	0.02	0.02	0.02	0.02	0.02
Cr_2O_3	0.17	0.19	0.28	0.41	0.34	0.28
NiO	0.30	0.26	0.29	0.25	0.25	0.22
LOI	10.36	8.86	5.99	7.37	4.26	9.52
Total	99.79	100.22	100.07	100.29	100.35	99.88
Trace elements (ppm)						
Sc	6.62	7.66	9.16	11.3	14.6	12.0
V	18.8	23.4	28.0	42.5	64.8	59.5
Cr	1321	1448	2030	2997	2436	2089
Ni	2626	2262	2443	2160	2091	1953
Co	128	117	123	113	112	106
Rb	0.22	0.20	0.32	0.15	0.19	0.28
Sr	8.52	66.6	23.1	0.83	0.09	2.10
Y	0.02	0.05	0.04	0.46	0.57	0.51
Zr	3.11*	n.m.	0.30	0.50	0.10	0.40
Nb	0.05	0.02	0.01	0.02	0.01	0.02
Sb	n.m.	n.m.	n.m.	n.m.	n.m.	n.m.
Cs	0.12	0.06	0.13	0.08	0.10	0.11
Ba	11.7	1.03	4.47	1.88	16.6	2.32
La	0.016	0.011	0.026	b.d.l.	0.025	0.011
Ce	0.081	0.025	0.059	0.023	0.055	0.023
Pr	0.005	0.002	0.004	b.d.l.	0.006	0.002
Nd	0.017	0.002	0.009	b.d.l.	0.016	0.010
Sm	0.002	0.001	0.003	0.011	0.008	0.005
Eu	0.003	0.001	0.002	0.006	0.006	0.003
Gd	0.002	0.006	0.004	0.029	0.026	0.018
Tb	0.000	0.001	0.001	0.008	0.008	0.007
Dy	0.004	0.011	0.011	0.069	0.083	0.069
Ho	0.001	0.003	0.003	0.019	0.023	0.020
Er	0.004	0.010	0.011	0.063	0.082	0.079
Tm	0.001	0.002	0.002	0.011	0.014	0.015
Yb	0.008	0.015	0.021	0.084	0.113	0.120
Lu	0.002	0.003	0.004	0.014	0.019	0.022
Hf	0.060	0.014	0.007	0.017	0.017	0.010
Ta	0.075	0.086	0.077	0.075	0.077	0.076
Pb	0.20	b.d.l.	b.d.l.	0.30	0.70	0.10
Th	0.012	0.006	0.008	0.002	0.010	0.006
U	0.090	0.046	0.014	0.004	0.033	0.034

Results

Petrography

The ultramafic body from Sedlice mainly consists of harzburgites (Fig. 2a from sample SE-15; SE-6b, SE-14); with lherzolites (Fig. 2b from sample SE-17b; SE-12) and dunites (samples SE-2, 3) rarely encountered. The intensively brecciated W/SW body margin was observed (Fig. 2c). The fractures of the brecciated peridotite margin are healed with secondary magnesite and calcite. The whole body is tectonically cracked into a system of blocks.

Microscopically, some ultramafics, exhibiting distinctly predominant olivine matrix (Fig. 2c), could be termed dunites. Typically mesh textured granular dunite (samples SE-2 and SE-3, Fig. 2c) is almost exclusively composed of slightly serpentinized olivine (~98–99 wt. %; from an incipient to moderate serpentinization stage) with a minimum of orthopyroxene grains (about 2–5 wt. %).

Harzburgites contain about 10–15 wt. % of orthopyroxene and less than 5 wt. % of clinopyroxene (samples SE-14 and SE-15). Orthopyroxene (1) is mostly porphyroclastic, often 1 to 2 mm in size, macroscopically visible. Harzburgite orthopyroxenes often show a strong replacement by chrysotile (Fig. 2d). Orthopyroxene porphyroclasts contain Spl inclusions (Fig. 2e,f).

Lherzolite is another rock type in the Sedlice peridotite (Fig. 2b). It usually has porphyric texture and contains more porphyroclastic Cpx (5–10 wt. %) besides Opx (~25 wt. %) (Fig. 3a,b). Enstatite, nearly colourless with a pinkish tinge in thin sections, mainly occurs as subhedral, sometimes euhedral porphyroclastic grains up to 2 mm in size (Opx_1 in Fig. 3a,b) with a distinct exsolution lamellae system of Cpx (Fig. 3c,d). Clinopyroxene,

Table 2: The chemical compositions of pyroxenes from the Sedlice peridotite body.

Sample	SE-6b	SE-6b	SE-6b	SE-6b	SE-6b	SE-6b	SE-6b	SE-10	SE-10	SE-10
Rock type	harzburgite	harzburgite	harzburgite	harzburgite	harzburgite	harzburgite	harzburgite	lherzolite	lherzolite	lherzolite
Mineral	Opx_1	Cpx_1	Opx_1	Cpx_1	Opx_1	Cpx_1	Cpx_1	Opx_1	Cpx_1	Opx_1
Analysis	an25	an26	an28	an27	an29	an30	an24	an8	an7	an13
(wt. %)										
SiO_2	56.85	53.13	56.23	52.78	56.41	53.00	53.47	55.47	51.34	54.82
TiO_2	0.05	0.13	0.03	0.12	0.05	0.15	0.13	0.05	0.13	0.05
Al_2O_3	2.94	3.31	3.40	3.98	3.11	3.48	3.55	4.45	4.93	4.72
Cr_2O_3	0.67	1.03	0.88	1.33	0.87	1.38	1.14	0.93	1.30	0.97
FeO	5.71	2.34	5.66	2.15	5.76	1.85	2.35	5.88	2.35	5.96
MnO	0.12	0.08	0.10	0.08	0.15	0.09	0.08	0.16	0.09	0.13
MgO	34.04	17.07	33.41	16.59	33.70	16.47	17.48	32.09	16.01	32.86
CaO	0.89	23.39	0.97	23.41	0.65	23.75	22.53	0.92	24.02	0.95
NiO	0.11	0.07	0.09	0.08	0.13	0.08	0.03	0.08	0.06	0.13
Na_2O	0	0.33	0.01	0.41	0.02	0.45	0.35	0	0.14	0.01
K_2O	0	0	0.01	0.02	0.01	0.01	0.01	0.01	0.01	0.01
Total	101.38	100.87	100.78	100.96	100.85	100.70	101.12	100.03	100.38	100.63
(a.p.f.u.)										
Si^{4+}	1.935	1.912	1.927	1.899	1.931	1.912	1.917	1.922	1.863	1.883
Al^{3+}	0.065	0.088	0.073	0.101	0.069	0.088	0.083	0.078	0.137	0.117
Fe^{3+}	0.000	0.000	0.000	0.000	0.000	0.000	0.000	0.000	0.000	0.000
Σ	2.000	2.000	2.000	2.000	2.000	2.000	2.000	2.000	2.000	2.000
Al^{3+}	0.053	0.052	0.065	0.068	0.057	0.060	0.066	0.104	0.073	0.074
Fe^{3+}	0.000	0.027	0.000	0.024	0.000	0.017	0.005	0.000	0.034	0.023
Ti^{4+}	0.001	0.004	0.001	0.003	0.001	0.004	0.003	0.001	0.003	0.001
Cr^{3+}	0.018	0.029	0.024	0.038	0.024	0.039	0.032	0.025	0.037	0.026
Mg^{2+}	0.928	0.889	0.911	0.867	0.918	0.879	0.893	0.870	0.852	0.875
Fe^{2+}	0.000	0.000	0.000	0.000	0.000	0.000	0.000	0.000	0.000	0.000
Mn^{2+}	0.000	0.000	0.000	0.000	0.000	0.000	0.000	0.000	0.000	0.000
Σ	1.000	1.000	1.000	1.000	1.000	1.000	1.000	1.000	1.000	1.000
Mg^{2+}	0.798	0.027	0.796	0.023	0.802	0.006	0.041	0.788	0.014	0.808
Fe^{2+}	0.163	0.044	0.162	0.041	0.165	0.038	0.066	0.170	0.037	0.148
Mn^{2+}	0.003	0.003	0.003	0.002	0.004	0.003	0.002	0.005	0.003	0.004
Ca^{2+}	0.033	0.902	0.036	0.902	0.024	0.918	0.865	0.034	0.934	0.035
Na^{+}	0.000	0.023	0.000	0.029	0.002	0.031	0.024	0.000	0.010	0.001
Σ	0.997	0.998	0.997	0.997	0.996	0.997	0.999	0.997	0.998	0.996
Wo	1.69	45.81	1.87	46.29	1.25	47.37	43.92	1.83	46.13	1.88
En	89.85	51.71	89.61	51.36	90.11	50.44	52.39	89.02	51.65	90.19
Fs	8.46	2.47	8.52	2.35	8.63	2.19	3.69	9.15	2.22	7.94

diopside and/or augite (Cpx_1, Fig. 3b) is colourless in thin section, sometimes slightly brownish to greenish, usually with Opx exsolution lamellae. Aggregates of Opx_2 and Cpx_2 (Fig. 3e,f) with anhedral shape and missing exsolution lamellae (with exception of a few grains) represent matrix pyroxene equivalents, surrounding Opx_1 and Cpx_1 porphyroclasts. Pyroxene can be partly replaced by metamorphic amphibole–tremolite, and spinel by chromite (Fig. 2g,h). The magmatic Spl is often reddish-brownish in thin section (Fig. 3e,f).

On the basis of calculated "modal" mineral compositions (Table 1), the studied ultramafic rocks can be classified as dunites (sample SE-2, 3 in Table 1 and 4 and Fig. 4), harzburgites (samples SE-6B, 14, 15 in Table 1 and Fig. 4) to lherzolites (samples SE-12 and 17B in Table 1 and Fig. 4). The Ol-Opx-Cpx classification diagram for peridotites (Fig. 4) with plotted representative samples from the Sedlice peridotite body was constructed on the basis of calculated wt. % of mineral phases (Table 1).

Mineral abbreviations used in text, tables and figures (with exception of MgChr) are after Whitney & Evans (2010). Amp = amphibole, Cpx = clinopyroxene, Chr = chromite, Ctl = chrysotile, Fo = forsterite, Ol = olivine, Opx = orthopyroxene, Spl = spinel, Srp = serpentine group, Mag = magnetite, MgChr = magnesiochromite, Tr = tremolite.

Microprobe mineral composition and whole-rock chemical data

The major element chemical compositions of minerals are listed in Tables 2–4.

The percentages of individual components of Wo, En and Fs in the Morimoto (1988) classification diagram for Ca-Mg-Fe pyroxenes (Quad) classifies Opx as enstatite and Cpx as diopside and augite (Fig. 5, Table 2). The Mg# of pyroxenes varies from ~0.90 to 0.92 in Opx and from ~0.92 to 0.95 in Cpx (Fig. 6). Al_2O_3 contents of Opx and Cpx range from 1 to 5.58 and from 0.81 to 5.45 wt. %, respectively (Fig. 6). Orthopyroxene and clinopyroxene in lherzolites have higher Al_2O_3 contents and lower Mg# [= Mg/(Mg + Fe) atomic ratio] than those in dunites and harzburgites. The Na_2O content is very low (< 0.5 wt. %) in Cpx.

The spinel-group minerals are the major accessory minerals in these rocks. According to Lindsley (1991) based on the

Table 2: *Continued.*

Sample	SE-10	SE-10	SE-10	SE-10	SE-15	SE-15	SE-15	SE-15	SE-15	SE-15	SE-15
Rock type	lherzolite	lherzolite	lherzolite	lherzolite	harzburgite	harzburgite	harzburgite	harzburgite	harzburgite	harzburgite	harzburgite
Mineral	Cpx_1	Opx_1	Cpx_1	Cpx_2	Opx_1	Opx_2	Opx_1	Opx_2	Cpx_2	Cpx_2	Cpx_2
Analysis	an12	an14	an15	an11	an4	an8	an21	an23	an3	an6	an16
(wt. %)											
SiO_2	51.24	55.15	51.67	52.52	56.92	57.15	57.46	57.40	53.56	53.83	54.38
TiO_2	0.15	0.02	0.11	0.10	0.02	0.01	0.01	0.03	0.02	0.00	0.01
Al_2O_3	5.15	4.84	4.77	4.04	1.36	1.02	1.14	1.23	1.09	0.81	1.13
Cr_2O_3	1.25	0.89	1.05	0.80	0.56	0.33	0.46	0.51	0.53	0.33	0.73
FeO	2.13	6.26	2.49	2.52	5.53	5.32	5.20	5.50	2.06	1.89	1.79
MnO	0.08	0.09	0.13	0.11	0.16	0.14	0.13	0.16	0.08	0.05	0.07
MgO	16.11	32.62	16.56	17.07	34.38	34.63	34.75	34.09	18.13	17.92	18.15
CaO	24.03	0.54	23.51	23.26	0.87	0.77	0.75	0.90	23.64	24.11	24.03
NiO	0.00	0.12	0.05	0.04	0.09	0.10	0.06	0.06	0.05	0.09	0.04
Na_2O	0.10	0.03	0.07	0.11	0	0	0.01	0	0.07	0.07	0.07
K_2O	0	0	0	0	0	0	0.01	0.01	0.01	0.01	0
Total	100.24	100.57	100.42	100.58	99.89	99.46	99.99	99.89	99.22	99.12	100.40
(a.p.f.u.)											
Si^{4+}	1.860	1.898	1.871	1.896	1.963	1.976	1.976	1.982	1.954	1.967	1.962
Al^{3+}	0.140	0.102	0.129	0.104	0.037	0.024	0.024	0.018	0.046	0.033	0.038
Fe^{3+}	0.000	0.000	0.000	0.000	0.000	0.000	0.000	0.000	0.000	0.000	0.000
Σ	2.000	2.000	2.000	2.000	2.000	2.000	2.000	2.000	2.000	2.000	2.000
Al^{3+}	0.080	0.094	0.075	0.068	0.018	0.017	0.022	0.032	0.001	0.002	0.011
Fe^{3+}	0.024	0.000	0.027	0.018	0.008	0.004	0.000	0.000	0.037	0.031	0.013
Ti^{4+}	0.004	0.001	0.003	0.003	0.001	0.000	0.000	0.001	0.001	0.000	0.000
Cr^{3+}	0.036	0.024	0.030	0.023	0.015	0.009	0.013	0.014	0.015	0.010	0.021
Mg^{2+}	0.857	0.881	0.866	0.889	0.958	0.970	0.965	0.954	0.946	0.957	0.955
Fe^{2+}	0.000	0.000	0.000	0.000	0.000	0.000	0.000	0.000	0.000	0.000	0.000
Mn^{2+}	0.000	0.000	0.000	0.000	0.000	0.000	0.000	0.000	0.000	0.000	0.000
Σ	1.000	1.000	1.000	1.000	1.000	1.000	1.000	1.000	1.000	1.000	1.000
Mg^{2+}	0.015	0.792	0.028	0.030	0.809	0.815	0.816	0.801	0.040	0.020	0.021
Fe^{2+}	0.041	0.180	0.049	0.058	0.151	0.150	0.150	0.159	0.026	0.027	0.041
Mn^{2+}	0.003	0.003	0.004	0.003	0.005	0.004	0.004	0.005	0.002	0.002	0.002
Ca^{2+}	0.934	0.020	0.912	0.900	0.032	0.029	0.028	0.033	0.924	0.944	0.929
Na^{+}	0.007	0.002	0.005	0.008	0.000	0.000	0.001	0.000	0.005	0.005	0.005
Σ	1.000	0.996	0.998	0.999	0.998	0.997	0.998	0.998	0.998	0.997	0.999
Wo	46.05	1.06	44.66	44.55	1.65	1.46	1.42	1.72	45.50	46.84	46.43
En	51.54	89.33	52.49	52.14	90.59	90.91	90.94	90.12	53.09	51.75	51.42
Fs	2.41	9.61	2.86	3.31	7.76	7.63	7.64	8.16	1.41	1.41	2.15

mineral chemical compositions (Table 3), they are classified as spinel, magnesiochromite and chromite end-members (Fig. 7a). The harzburgites contain only magnesiochromite and chromite, whereas lherzolites also preserve the spinel end member. Chromite grains are round-shaped or euhedral, sometimes weakly cataclastic. They are accumulated along mineral grain boundaries, in serpentine veins in the form of mineral inclusions or dispersed as small and/or large grain clusters. Magnetite is the youngest of the spinel-group minerals. It occurs in the form of large patches around primary reddish spinel, or it kneads the cataclastic chromite in the form of veins. A single grain of andradite garnet was found in the more altered part of harzburgite.

Spinel compositions vary widely between samples. Spinel in harzburgites is represented by rounded, usually euhedral to subhedral chromite and vermicular magnesiochromite. It is systematically higher in Cr#[=Cr/(Cr+Al) atomic ratio; Cr#=0.58–0.85] and lower in Mg#[=Mg/(Mg+Fe^{2+}) atomic ratio; Mg#=0.37–0.60] than that in lherzolites, represented by reddish spinel (Cr#=0.14–0.37; Mg#=0.66–0.79; Fig. 7a). The TiO_2 content is low (<0.22 wt. %; Fig. 7b) in all cases, only the sample SE-14 represented by harzburgite has significantly higher TiO_2 contents in the range from 0.18 to 0.21 compared to other samples. Cr# in Spl/Fo in Ol diagram (Fig. 8a) and Cr_2O_3/Al_2O_3 Spl diagram (Fig. 8b) plot most of the samples in the Mantle-array. The only exception is sample SE-3 containing Spl with an increased Cr#, which is compatible with the dunite as the hosting rock.

Olivine is the most representative rock-forming mineral with forsterite content ranging from 89.0 to 91.4 in lherzolites, and from 90.0 to 92.0 in harzburgites. The NiO content of olivine ranges from 0.31 to 0.47 wt. % in harzburgites, and from 0.36 to 0.51 wt. % in lherzolites (Table 4). The relationship between the Fo content of olivine and Cr# of spinel shows that all lherzolites and harzburgites plot into the Ol-Spl mantle array (OSMA), a residual mantle trend of spinel peridotite (Arai 1987, 1994; Fig. 8a). Olivine composition is in correlation with spinel; spinel Cr# increases and spinel Mg# decreases as olivine Fo increases in the OSMA (Choi et al. 2008).

The Primitive Mantle (PM) normalized rare earth element concentrations from the whole-rock analyses are plotted in Fig. 9. They show a decrease in REE as a whole, but a relative increase in LREE, particularly Ce and La, in comparison with HREE. Three to four samples exhibit a positive Eu anomaly.

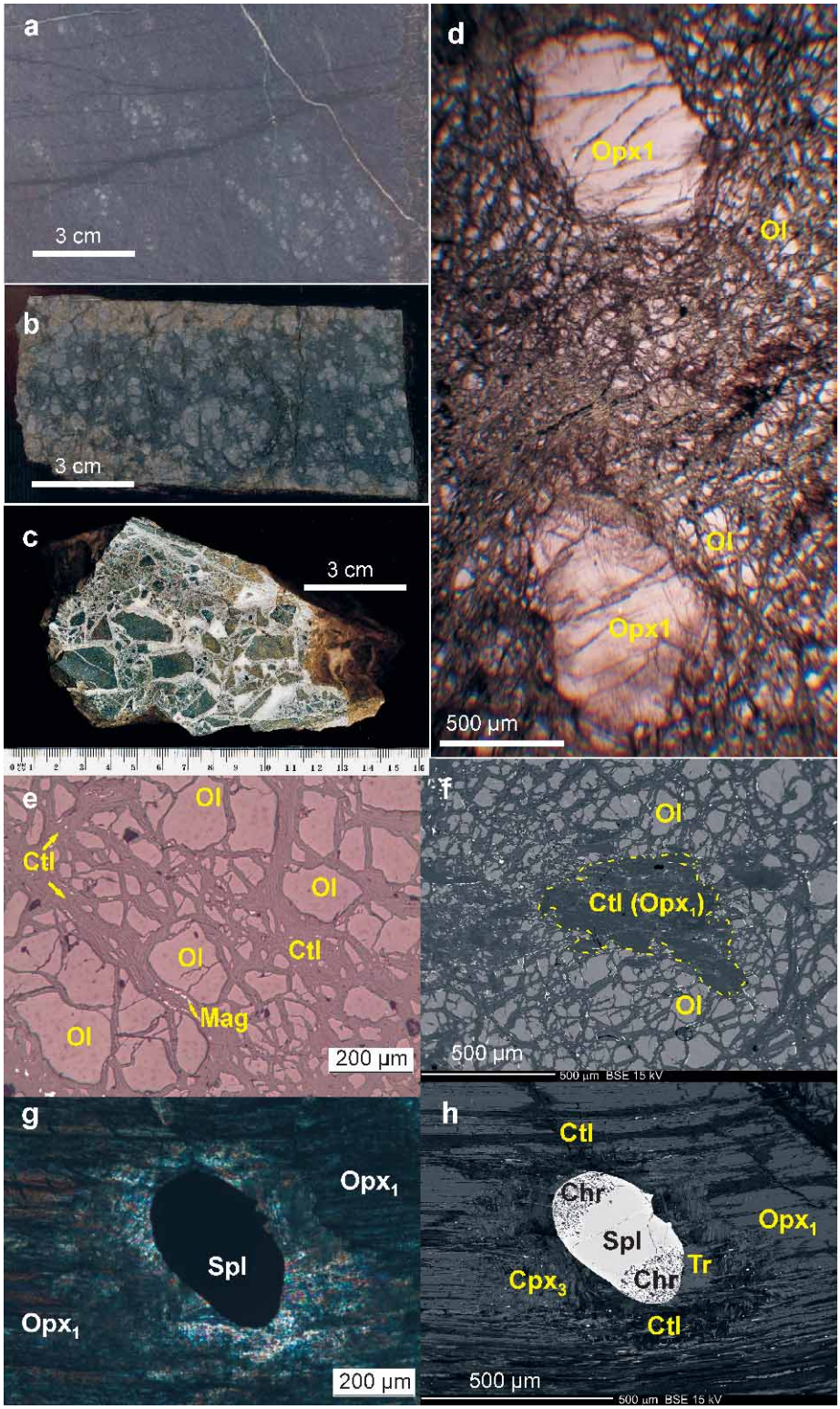

Fig. 2. a — Serpentinized harzburgite (sample SE-15) from Sedlice peridotite with preserved pyroxene porphyroclasts; **b** — Slightly serpentinized lherzolite from Sedlice peridotite (sample SE-17b); **c** – Tectonic breccia composed of harzburgite angular fragments cemented by carbonates — calcite and magnesite; **d** — Photomicrograph (cross-polarized light) of harzburgite (sample SE-15) with Opx_1 porphyroclasts in olivine-rich matrix; **e** — Photomicrograph (reflected light) of granular dunite (sample SE-3) from Sedlice locality with typical mesh textured serpentine minerals forming veins surrounding the relic center of olivine grains; **f** — BSE image of serpentinized dunite (sample SE-3) with outlined boundary of rare orthopyroxene (1); **g** — Photomicrograph (cross-polarized light); **h** — BSE image of spinel rim dissolution-reprecipitation replacement (Putnis 2009) by metamorphic chromite in host orthopyroxene (1) porphyroclast in Sedlice serpentinized harzburgite (sample SE-6b). Orthopyroxene partly replaced by metamorphic Srp and Tr.

Table 3: The chemical compositions of spinel group minerals from the Sedlice peridotite body.

Sample	SE-3	SE-3	SE-6b	SE-6b	SE-6b	SE-12	SE-12	SE-12	SE-14	SE-14	SE-14	SE-15	SE-15	SE-17b	SE-17b	SE-17b
Rock type	dun	dun	harz	harz	harz	lherz	lherz	lherz	harz	harz	harz	harz	harz	lherz	lherz	lherz
Mineral	Chr	Chr	Spl	Spl	Spl	Spl	Spl	Spl	MgChr	MgChr	MgChr	MgChr	Chr	Spl	Spl	Spl
Ana No.	1	2	9	21	59	60	3	4	8	11	12	13	14	15	2	3	8
(wt. %)																	
TiO_2	0.05	0.06	0.05	0.07	0.08	0.05	0.02	0.02	0.06	0.21	0.19	0.20	0.04	0.03	0.05	0.08	0.07	0.05
Al_2O_3	7.40	7.25	7.55	36.32	36.59	38.74	46.65	55.08	44.45	21.03	21.14	21.20	19.03	21.52	22.08	49.39	50.38	51.67
V_2O_3	0.21	0.29	0.34	0.12	0.11	0.12	0.16	0.12	0.12	0.21	0.22	0.22	0.24	0.26	0.19	0.16	0.13	0.13
Cr_2O_3	62.53	61.50	62.24	31.45	32.66	31.10	21.15	12.93	23.42	47.60	48.15	47.97	50.27	45.82	45.86	19.54	18.90	16.64
FeO	21.49	22.11	22.17	14.99	14.78	14.64	12.65	10.86	13.17	17.52	17.70	17.65	18.40	20.80	21.17	11.18	11.44	12.03
MnO	0.56	0.58	0.58	0.25	0.21	0.22	0.19	0.16	0.18	0.37	0.37	0.41	0.39	0.44	0.44	0.16	0.17	0.17
MgO	7.99	7.38	7.73	15.45	15.48	15.89	17.64	19.39	17.74	12.64	12.46	12.33	11.94	10.27	9.98	18.49	18.81	18.66
NiO	0	0.071	0	0.15	0.14	0.15	0.24	0.30	0.22	0.05	0.10	0.06	0.06	0	0	0.20	0.27	0.15
ZnO	0.21	0.14	0.24	0.14	0.19	0.14	0.21	0.24	0.21	0.10	0.08	0.19	0.21	0.30	0.43	0.25	0.18	0.23
Total	100.44	99.39	100.91	98.92	100.24	101.06	98.91	99.10	99.56	99.73	100.43	100.21	100.57	99.46	100.20	99.43	100.35	99.73
(a.p.f.u.)																		
Ti^{4+}	0.001	0.001	0.001	0.002	0.002	0.001	0.000	0.000	0.001	0.005	0.004	0.005	0.001	0.001	0.001	0.002	0.001	0.001
Al^{3+}	0.294	0.293	0.299	1.236	1.232	1.283	1.510	1.710	1.442	0.769	0.769	0.773	0.700	0.800	0.815	1.570	1.582	1.623
V^{3+}	0.006	0.008	0.009	0.003	0.003	0.003	0.004	0.003	0.003	0.005	0.005	0.005	0.006	0.007	0.005	0.003	0.003	0.003
Cr^{3+}	1.668	1.665	1.655	0.718	0.738	0.691	0.459	0.269	0.510	1.168	1.175	1.174	1.240	1.142	1.135	0.417	0.398	0.351
Fe^{3+}	0.036	0.041	0.044	0.044	0.028	0.024	0.031	0.021	0.047	0.059	0.052	0.048	0.059	0.058	0.048	0.012	0.019	0.025
Fe^{2+}	0.570	0.592	0.579	0.318	0.325	0.320	0.260	0.218	0.256	0.396	0.405	0.409	0.421	0.491	0.506	0.240	0.236	0.243
Mn^{2+}	0.016	0.017	0.017	0.006	0.005	0.005	0.004	0.004	0.004	0.010	0.010	0.011	0.010	0.012	0.012	0.004	0.004	0.004
Mg^{2+}	0.402	0.377	0.388	0.665	0.659	0.666	0.722	0.761	0.728	0.585	0.573	0.569	0.555	0.483	0.466	0.743	0.747	0.741
Ni^{2+}	0.000	0.002	0.000	0.003	0.003	0.003	0.005	0.006	0.005	0.001	0.002	0.001	0.002	0.000	0.000	0.004	0.006	0.003
Zn^{2+}	0.005	0.004	0.006	0.003	0.004	0.003	0.004	0.005	0.004	0.002	0.002	0.004	0.005	0.007	0.010	0.005	0.004	0.004
Total	2.999	3.000	2.999	2.998	3.000	3.000	3.000	2.997	2.999	2.999	2.998	2.999	2.999	2.999	2.998	3.000	2.999	2.999
Mg#	0.414	0.389	0.401	0.677	0.670	0.676	0.735	0.777	0.740	0.596	0.586	0.582	0.569	0.496	0.479	0.756	0.760	0.753
Cr#	0.850	0.851	0.847	0.367	0.374	0.350	0.233	0.136	0.261	0.603	0.604	0.603	0.639	0.588	0.582	0.210	0.201	0.178

Discussion

The dunites represent the most refractory residual mantle rocks observed in the Sedlice peridotite body in association with prevailing harzburgites and exclusively with lherzolites. The studied rocks from this body are characterized by a wide range of Cr# (from 0.14 to 0.85) in Spl. The relationship between Cr# of spinel and Fo of olivine indicates that studied rocks are within the OSMA (Arai 1987, 1994) and represent residual equivalents of a mantle peridotite which compositionally reveal a wide range of melt extraction derived by partial melting of a more fertile mantle peridotite (Fig. 8a,b). The Fo content of olivine and Cr# of spinel do not change during subsolidus recrystallization (Ozawa 1988; Arai 1994). The Cr# of spinel-group minerals is progressively increasing with partial melting degree, which, on the other hand, reduces the original Al contents in Spl and Opx, and the host rock (Dick & Bullen 1984; Arai 1994; Ohara & Ishi 1998). Therefore such a wide range of Cr# in spinel in our rocks is good indicator of a wide range of degrees of partial melting. Based on the cited concepts, the chemical compositions of chromian spinels (Cr-Spl) are plotted in various discrimination diagrams. The spinel data for lherzolite (SE-12, SE-17b) and harzburgite (SE-6b, SE-14, SE-15) are plotted within the mantle array on an Al_2O_3/Cr_2O_3 diagram (Fig. 8b). In the diagram Mg#/Cr# (Fig. 7a) the most Cr-spinels from lherzolite (i.e. plot of the lowest Cr# values; samples SE-12 and SE-17b) indicate its relatively undepleted nature. On the other hand, the Cr-spinel data of refractory harzburgite (samples SE-14 and SE-15) indicates depleted character. The highest depletion of the mantle rocks is inferred in an arc tectonic setting and/or in a supra-subduction zone environment (e.g. Arai 1994; Choi et al. 2008). The Cr# of spinel in abyssal peridotites collected from mid-ocean ridges is less than 0.6 (Tamura & Arai 2006). Our samples have mostly comparable (SE-15, SE-14), but also slightly higher (SE-3) values (Figs. 7, 8). The TiO_2 content is extremely low in arc/back-arc magma, intermediate in mature mid-oceanic ridge magma and high in intra-plate magma (Arai 1992). The spinel TiO_2 contents plotted in Fig. 7b record low concentrations in all samples. The diagram Mg# versus Al_2O_3 content in pyroxenes

(Fig. 6) shows differences in composition between lherzolite and harzburgite most likely due to variable degrees of their depletion.

Trace rare earth element concentrations from whole-rock analyses are plotted in Fig. 9 and exhibit a depletion trend in harzburgites, corresponding to their refractory origin in relationship to more fertile lherzolites. The basic trend in PM normalized REE patterns (Fig. 9a) indicates a depleted rock-suite, however an increase in LREE to HREE is similar to the Dobšiná meta-harzburgites (Putiš et al. 2012), likely indicating an influence of metamorphic fluids during serpentinization. The whole-rock positive Eu anomaly suggests

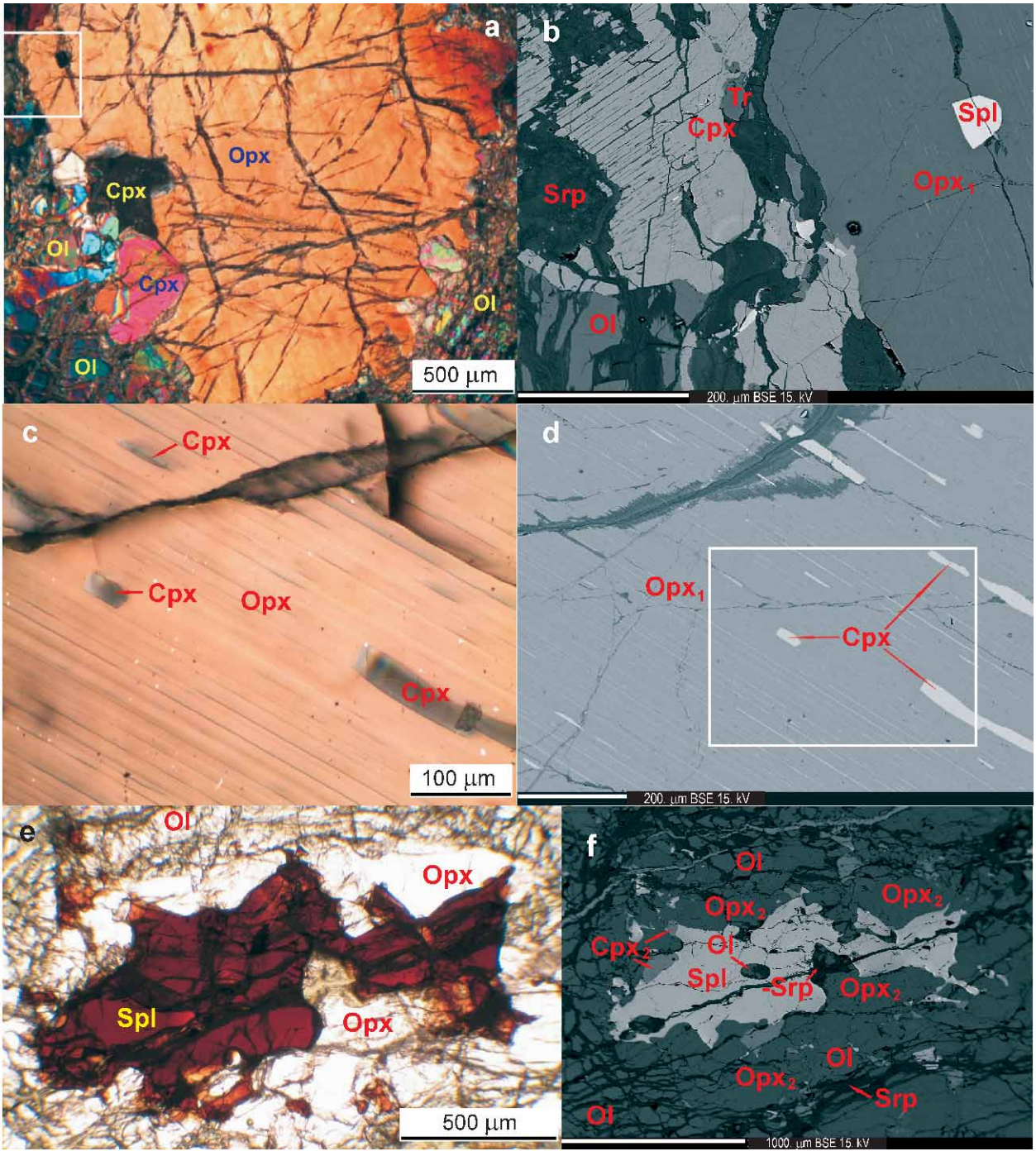

Fig. 3. Photomicrographs of a slightly serpentinized Spl lherzolite (samples SE-12) from Sedlice peridotite. **a** — Photomicrograph (cross-polarized light) of porphyroclastic Opx_1 with Spl inclusion (in the frame); **b** — BSE image of Spl inclusion in Opx_1 (from image in **a**); **c** — Photomicrograph (cross-polarized light) of exsolved clinopyroxene lamellae in host Opx_1 (a BSE image detail in **d** frame); **d** — BSE image detail of **c** in the frame; **e** — Photomicrograph (plain-polarized light) of brown-reddish spinel in Opx_2–Cpx_2 aggregate; **f** — BSE image of spinel from **e**.

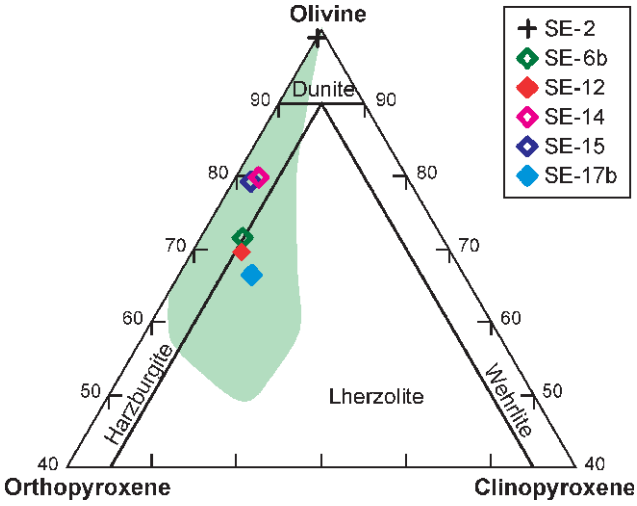

Fig. 4. Classification diagram for peridotites with representative samples from Sedlice peridotite body plotted and calculated on the basis of primary mineral phases and whole-rock chemical compositions (mineral quantities are calculated in wt. %; Table 1). The pale green area represents the most common compositions of peridotites in the upper part of the Earth's mantle (partly adapted from Bodinier & Godard (2007)).

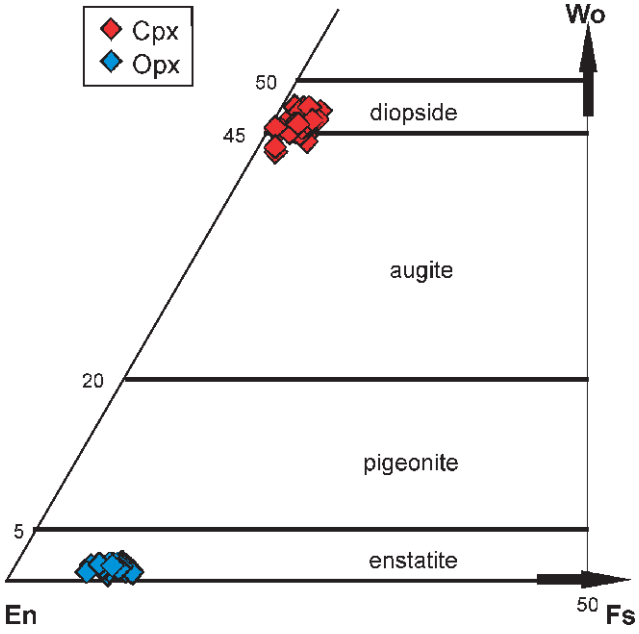

Fig. 5. Pyroxenes from Sedlice peridotite in the Morimoto (1988) classification.

Table 4: Olivine chemical compositions from the Sedlice peridotite body.

Sample	SE-3	SE-6b	SE-14	SE-15	SE-12	SE-17b
Rock type	dun	harz	harz	harz	lherz	lherz
# of analyses	6	16	6	7	5	4
(wt. %)						
SiO_2	41.37	40.98	41.61	41.38	40.98	41.38
$FeO_{(tot)}$	8.28	8.82	8.49	8.03	9.01	9.05
MnO	0.12	0.13	0.11	0.12	0.13	0.14
MgO	50.33	49.42	50.22	50.04	49.67	49.27
CaO	0.01	0.03	0.01	0.02	0.03	0.25
NiO	0.40	0.41	0.42	0.39	0.42	0.42
Total	100.56	99.87	100.92	100.06	100.33	100.60
Mg#	0.92	0.91	0.91	0.92	0.91	0.91
Fo	91.18	90.50	90.95	91.37	90.35	89.98

Table 5: The chemical compositions of metamorphic minerals from the Sedlice peridotite body.

Sample	SE-3	SE-6b	SE-6b	SE-10	SE-6b	SE-6b	SE-15	SE-17b
Rock type	dun	harz	harz	lherz	harz	harz	harz	lherz
Mineral	Srp	Srp	Srp	Srp	Cpx_3	Cpx_3	Tr	Tr
Ana No.	5	11	73	10	32	34	19	9
(wt. %)								
SiO_2	43.49	42.66	36.83	40.27	54.78	55.09	57.23	54.78
TiO_2	0	0	0.03	0	0.03	0.04	0.01	0.19
Al_2O_3	0.06	1.55	1.96	0.17	1.24	0.92	1.22	3.92
Cr_2O_3	0.01	0.64	0.83	0.00	0.35	0.27	0.50	0.77
FeO	1.63	3.20	6.35	6.66	2.01	1.57	1.95	2.18
MnO	0.03	0.08	0.19	0.25	0.12	0.13	0.04	0.04
MgO	42.35	37.89	36.23	35.90	21.29	20.38	23.29	21.90
CaO	0.02	0.11	0.06	0.23	19.08	22.12	13.50	13.28
NiO	0.16	0.02	0.10	0.36	0.02	0.15	0.11	0.08
Na_2O	0	0.09	0	0.01	0.55	0.30	0.13	0.64
K_2O	0.02	0.06	0.02	0.04	0.18	0.11	0.01	0.03
Cl	0.03	0.05	0.46	0.13	0	0	0.04	0.05
Total	87.80	86.36	83.06	84.01	99.64	101.07	98.04	97.85

substitution of $Eu^{2+}$for Ca^{2+}, likely in tremolite (in the B site) or rare carbonates. The trace element mobility is also documented in spider diagram (Fig. 9b) showing a relative increase in Cs, Ba, U, Ta, Ce, Sr, Zr, Hf and Ti. The main difference between the less and more depleted rocks exhibit HREE and Ti, which are increased in (less depleted) lherzolites.

From this point of view, the harzburgites from the Sedlice peridotite body could be genetically bound to an abyssal mantle peridotite (e.g. Bodinier & Godard 2007). Some of the Spl analyses at the boundary of the mantle array could indicate either a higher melting degree, or a later influence of metamorphic fluids, or both.

The studied peridotite body exhibits features of low-temperature metamorphic overprint. Metamorphic mineral assemblage contains chrysotile, tremolite, andradite garnet, Cr-spinel to chromite and magnetite, an increase of fayalite component in olivine, and rare carbonate. This might be related to serpentinization and a weak rodingitization in an accretionary wedge, resembling the Meliatic Bôrka Nappe serpentinized and rodingitized harzburgites (Putiš et al. 2012; Li et al. 2014). Because of practically missing high-pressure metamorphic overprint, characteristic for the Meliatic Bôrka blueschist-bearing nappe (with antigorite-clinopyroxene-pargasite-bearing meta-harzburgites, Putiš et al. 2012), this body could indicate an obduction process and incorporation into an accretionary wedge due to closure of the Neotethyan Meliatic (Triassic–Jurassic) oceanic back-arc basin in the Late Jurassic (Dallmeyer et al. 1996; Mock et al. 1998; Faryad et al. 2005; Putiš et al. 2011).

The Sedlice body could be an olistolith, which slided into the Paleogene sediments from the Bôrka Nappe, overlying the Central Western Carpathians

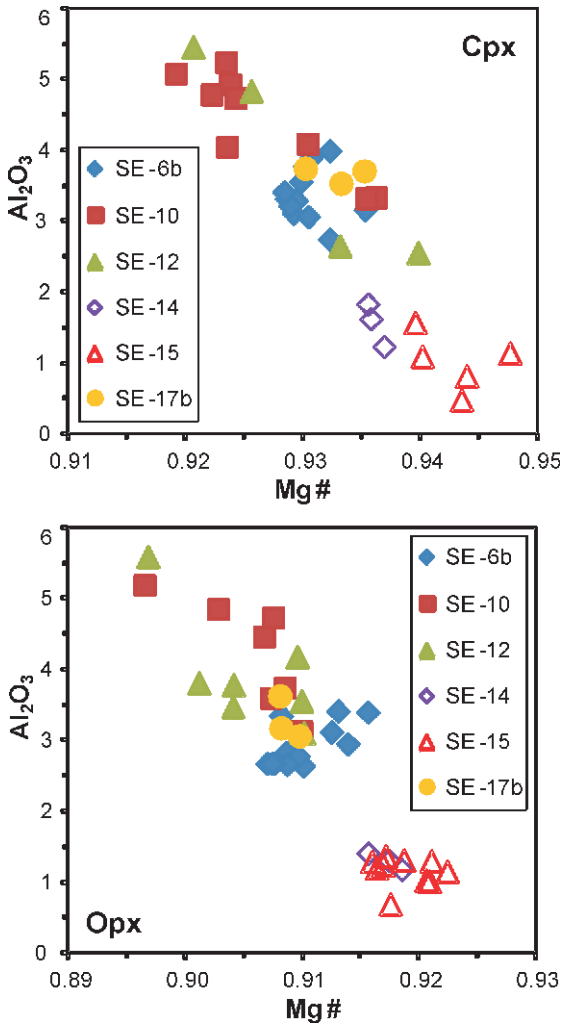

Fig. 6. Plot of Mg#[=Mg/(Mg+Fe) atomic ratio] versus Al_2O_3 contents (wt. %) in monoclinic and rhombic pyroxenes from Sedlice peridotite.

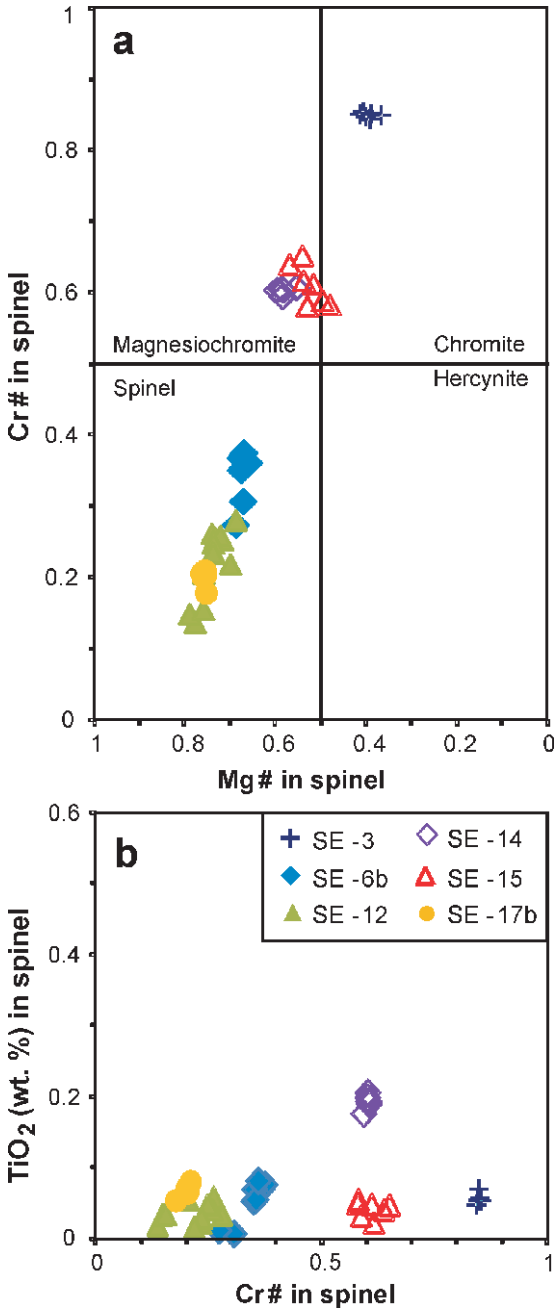

Fig. 7. Spinel compositional variations in the peridotite body from Sedlice. **a** — Relationship between Cr#[=Cr/(Cr+Al) atomic ratio] and TiO_2 content; **b** — Relationship between Mg#[=Mg/(Mg+Fe^{2+}) atomic ratio] and Cr#. The individual spinel-group end-member mineral terminology is after Lindsley (1991).

orogenic wedge since the Late Cretaceous. Alternatively it could be a younger tectonic protrusion body from the underlying basement units, most likely from the Meliatic Bôrka Nappe, which originated after covering by the Paleogene basal and younger flysch sediments. Nevertheless, the surface occurrences of the metaperidotites of the Bôrka Nappe are not so far away — along the Gemeric/Veporic Late Cretaceous tectonic boundary, to the south (SW) of the Central-Carpathian Paleogene Basin (Fig. 1). The brecciation of the body margin healed by magnesite and calcite postdates pervasive and relatively higher-temperature serpentinization most likely in an accretionary wedge. Therefore the brecciation might reflect an interaction of CO_2-rich water with the body margin within the sedimentary basin.

Conclusions

The spinel peridotite from Sedlice comprises mainly depleted harzburgites accompanied by lherzolites and dunites, which formed in a spinel stability field mantle environment. The studied samples point to a wide range of depletion. By composition, the lherzolites are close to fertile spinel lherzolites. The harzburgites represent depleted mantle rocks or residual equivalents formed by various degree of partial melting of more fertile lherzolites. The depletion is recorded in their refractory lithology and mineral chemical compositions. Cumulates, the expected derivatives formed by magmatic differentiation or a higher degree partial melting were not found in this body.

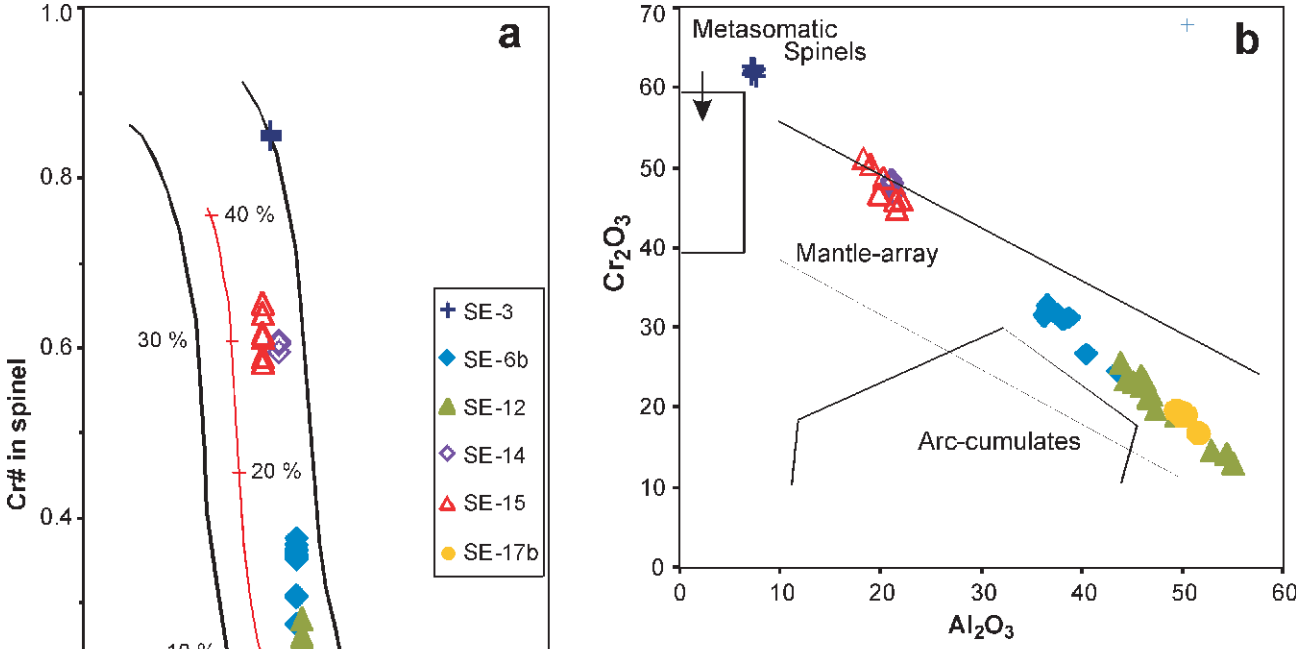

Fig. 8. **a** — Compositional relationship between Fo[=Mg/((Mg+Fe+Ca+Ni)/100) atomic ratio] content of olivine and Cr#[=Cr/(Cr+Al) atomic ratio] of spinel from the Sedlice peridotite body. OSMA (Olivine–Spinel Mantle Array) is a spinel peridotite residual trend and with melting trend (red curved line annotated by melting %) are from Arai (1987, 1994). *FMM* — fertile MORB mantle; **b** — Discrimination diagram Al_2O_3 versus Cr_2O_3 (wt. %) with plotted spinels from the Sedlice peridotite body (after Franz & Wirth 2000).

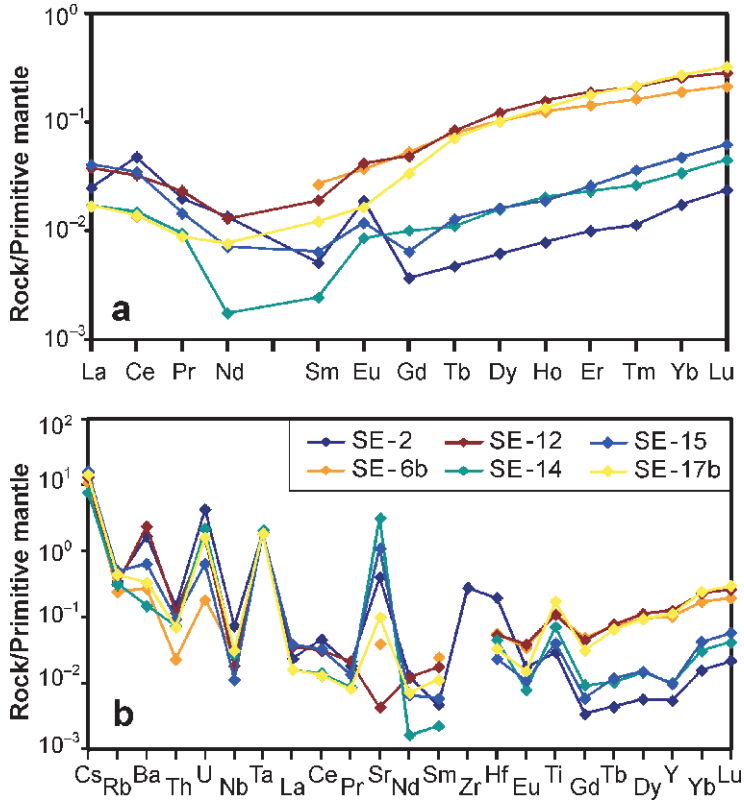

Fig. 9. **a** — Primitive Man; **b**— Spider diagram from Sedlice peridotite.

The PM normalized REE patterns indicate a depleted rock-suite, however an increase in LREE to HREE most likely reveals an influence of metamorphic fluids due to serpentinization. The whole-rock positive Eu anomaly might have been caused by substitution of Eu^{2+} for Ca^{2+} in tremolite or rare carbonates.

The low-temperature metamorphic mineral assemblage of peridotite body contains chrysotile, tremolite, rare andradite garnet, Cr-spinel to chromite and magnetite, and rare carbonate; this could also be determined by an increase of the fayalite component in olivine. These features resemble the Meliatic meta-harzburgites in the Western Carpathians.

The Sedlice peridotite body most likely formed from the Meliatic Bôrka Nappe slices and currently appears to be a protrusive(?) body within the Central-Carpathian Paleogene sediments. The brittle fractures healed by magnesite and calcite crosscut the serpentinized peridotite body and

therefore may represent a younger carbonate mineralization of unclear age.

Acknowledgments: This work was supported by the APVV-0081-10 and VEGA-1/0255/11 scientific Grants (M.P.). Doc. RNDr. Pavel Fejdi, CSc. deserves special thanks for grateful suggestions and helpful experiences. We honour his memory. The suggestions of J. Ulrych, D. Hovorka and one anonymous reviewer are greatly acknowledged. We also thank M. Styan for reviewing the English content.

References

Arai S. 1987: An estimation of the least depleted spinel peridotite on the basis of olivine–spinel mantle array. *Neu. Jb. Miner. Monat.* 8, 347–354.

Arai S. 1994: Characterization of spinel peridotites by olivine–spinel compositional relationships: review and interpretation. *Chem. Geol.* 113, 191–204.

Biely A., Bezák V., Elečko M., Gross P., Kaličiak M., Konečný V., Lexa J., Mello J., Nemčok J., Potfaj M., Rakús M., Vass D., Vozár J. & Vozárová A. 1996: Geological map of Slovakia, 1:500,000. *State Geological Institute of Dionýz Štúr Publishers*, Bratislava.

Bodinier J.L. & Godard M. 2007: Orogenic, ophiolitic, and abyssal peridotites. In: Carlson R.W. (Ed.): Treatise on geochemistry. Vol. 2. *Elsevier*, Amsterdam, 1–73.

Brandon M.T. 2004: The Cascadia subduction wedge: the role of accretion, uplift, and erosion. In: van der Pluijm B.A. & Marshak S. (Eds.): Earth structure: An introduction to structural geology and tectonics. 2nd ed. *WCB/McGraw Hill Press*, 566–574.

Burnham M., Meisel T. & Kriete C. 2010: OKUM and MUH-1: two new IAG-certified ultramafic rock reference materials. *Geochim. Cosmochim. Acta* 74, Suppl 1, A129.

Cambel B. 1951: Ultrabasic rock from Sedlice and serpentines of the closest surrounding. [Ultrabázická hornina od Sedlíc a hadce najbližšieho okolia.] *Geol. Zbor. Slovak. Akad. Vied* 2, 1–91 (in Slovak).

Choi S.H., Shervais J.W. & Mukasa S.B. 2008: Supra-subduction and abyssal mantle peridotites of the Coast Range ophiolite, California. *Contr. Mineral. Petrology* 156, 551–576.

Dallmeyer R.D., Neubauer F., Handler R., Fritz H., Müller W., Pana D. & Putiš M. 1996: Tectonothermal evolution of the internal Alps and Carpathians: Evidence from $^{40}Ar/^{39}Ar$ mineral and whole-rock data. *Eclogae Geol. Helv.* 89, 203–227.

Dick H.J.B. & Bullen T. 1984: Chromian spinal as a petrogenetic indicator in abyssal and alpine-type peridotites and spatially associated lavas. *Contr. Mineral. Petrology* 86, 54–76.

Faryad S.W., Spišiak J., Horváth P., Hovorka D., Dianiška I. & Jósza S. 2005: Petrological and geochemical features of the Meliata mafic rocks from the sutured Triassic oceanic basin, Western Carpathians. *Ofioliti* 30, 27–35.

Fejdi P. & Kolník B. 1988: Pyroxene geothermometry and geobarometry of ultrabasic body near Sedlice, Eastern Slovakia. [Pyroxénová geotermometria geobarometria ultrabázického telesa pri Sedliciach.] *Miner. Slovaca* 20, 149–159 (in Slovak).

Franz L. & Wirth R. 2000: Spinel inclusions in olivine of peridotite xenoliths from TUBAF seamount (Bismark Archipelago/Papua New Guinea): evidence for the thermal and tectonic evolution of the oceanic lithosphere. *Contr. Mineral. Petrology* 140, 283–295.

Gnojek P. & Kubeš P. 1991: Magnetometric evidence to the Sedlice ultramafic body. [Svědectví magnetometrie o ultrabázickém tělese u Sedlíc.] *Miner. Slovaca* 23, 161–164 (in Czech).

Hovorka D. 1977: Geochemistry of the West Carpathian Alpine-type ultramafites. *Veda, Nauka o Zemi, Geol.* 12, 1–148.

Hovorka D., Dubíková K., Gerthoferová H., Šamajová E. & Turan J. 1980: Serpentine — group minerals of the Western Carpathians ultramafics. I. Bodies of the Gemeride Mesozoic. *Miner. Slovaca* 12, 481–506.

Hovorka D., Ivan P., Jaroš J., Kratochvíl M., Reichwalder P., Rojkovič I., Spišiak J. & Turanová L. 1985: Ultramafic rocks of the Western Carpathians. *GÚDŠ*, Bratislava, 1–253.

Jaroš J., Kratochvíl M. & Zlocha J. 1981: Mesoscopic structural analysis of serpentinite bodies in the Spišsko-gemerské rudohorie Mts. (Eastern Slovakia). [Drobnoštruktúrna analýza vnútornej stavby serpentinitových telies v Spišsko-gemerskom rudohorí.] *Miner. Slovaca* 13, 527–548 (in Slovak).

Kantor J. 1955: Ore minerals of Spiš-Gemeric serpentinites (awaruite, heazlewoodite etc.). [Rudné minerály Spišsko-Gemerských serpentinitov (awaruit, heazlewoodit atď.).] *Geol. Zbor. Slov. Akad. Vied* 6, 1–302 (in Slovak).

Li X.-H., Putiš M., Yang Y.-H., Koppa M. & Dyda M. 2014: Accretionary wedge harzburgite serpentinization and rodingitization constrained by perovskite U/Pb SIMS age, trace elements and Sm/Nd isotopes: case study from the Western Carpathians, Slovakia. *Lithos* 205, 1–14.

Lindsley D.H. 1991: Oxide minerals: petrologic and magnetic significance. *Rev. in Mineralogy* 25, 1–509.

Marschalko R. 1966: Geology and sedimentology of marginal flysch lithophacies from the central Carpathians (Šariš highlands). [Geológia a sedimentológia flyšových okrajových litofácií centrálnych Karpát (Šarišská hornatina).] *Sbor. Geol. Vied, Západ. Karpaty* 5, 1–9 (in Slovak).

McDonough W.F. & Sun S. 1995: The composition of the Earth. *Chem. Geol.* 120, 223–253.

Meisel T., Schöner N., Paliulionyte V. & Kahr E. 2002: Determination of rare earth elements (REE), Y, Th, Zr, Hf, Nb and Ta in geological reference materials G-2, G-3, SCo-1 and WGB-1 by sodium peroxide sintering and ICP-MS. *Geostand. Newsl.* 26, 53–61.

Mikuš T. & Spišiak J. 2007: Chemical composition and alter ation of Cr-spinels from Meliata and Penninic serpentinized peridotites (Western Carpathians and Eastern Alps). *Geologica Q.* 51, 257–270.

Mock R., Sýkora M., Aubrecht R., Ožvoldová L., Kronome B., Reichwalder P. & Jablonský J. 1998: Petrology and petrography of the Meliaticum near the Meliata and Jaklovce villages, Slovakia. *Slovak Geol. Mag.* 4, 223–260.

Morimoto N., Fabries J., Ferguson A.K., Ginzburg I.V., Ross M., Seifert F.A. & Zussman J. 1988: Nomenclature of pyroxenes. *Amer. Mineral.* 73, 1123–1133.

Plašienka D., Grecula P., Putiš M., Kováč M. & Hovorka D. 1997: Evolution and structure of the Western Carpathians: an overview. In: Grecula P., Hovorka D. & Putiš M. (Eds.): Geological evolution of the Western Carpathians. *Miner. Slovaca, Geocomplex*, Bratislava, 1–24i.

Putiš M., Koppa M., Snárska B., Koller F. & Uher P. 2012: The blueschist-associated perovskite–andradite-bearing serpentinized harzburgite from Dobšiná (the Meliata Unit), Slovakia. *J. Geosci.* 58, 221–240.

Putiš M., Radvanec M., Sergeev S., Koller F., Michálek M., Snárska B., Koppa M., Šarinová K. & Németh Z. 2011: Metamorphosed succession of cherty shales with basalt and diastrophic breccia in olistolith of the Meliatic Jurassic accretion wedge near Jaklovce (Slovakia), dated on zircon (U–Pb SIMS SHRIMP). *Miner. Slovaca* 43, 1–18.

Putnis A. 2009: Mineral replacement reactions. *Rev. Mineral. Geochem.* 70, 87–124.

Radvanec M. 2000: P-T path and exhumation of ultra-high pressure

metamorphosed peridotite at Jaklovce on the north of Gemericum and on the locality Skalka at Sedlice northward of the zone Branisko–Čierna hora Mts. (Western Carpathians, Slovakia). [P-T dráha exhumácie ultravysokotlakovo metamorfovaného peridotite neďaleko Jakloviec na severe gemerika a na lokalite Skalka pri Sedliciach na sever od pruhu Branisko–Čierna hora.] *Miner. Slovaca* 32, 439–458 (in Slovak).

Rojkovič I. 1985: Ore mineralization of ultramafic bodies in Western Carpathians. [Rudná mineralizácia ultramafických telies Západných Karpát.] *Veda, SAV*, Bratislava, 1–63 (in Slovak).

Rojkovič I. & Boronichin V.A. 1982: Sulphidic nickel-cobalt-iron ores in ultramafic rocks of the Western Carpathians. [Sulfidická Ni-Co-Fe mineralizácia v ultramafických horninách Západných Karpát.] *Miner. Slovaca* 14, 41–59 (in Slovak).

Rojkovič I. & Hovorka D. 1979: Relation of ore mineralization to geochemistry of the West Carpathian ultramafic massifs. *Geol. Zbor. Geol. Carpath.* 30, 449–462.

Rojkovič I., Hovorka D. & Krištín J. 1978: Spinel group minerals in the West Carpathians ultrabasic rocks. *Geol. Zbor. Geol. Carpath.* 29, 1–253.

Scambelluri M., Fiebig J., Malaspina N., Müntener O. & Pettke T. 2004: Serpentinite subduction: implications for fluid processes and trace-element recycling. *Int. Geol. Rev.* 46, 595–613.

Stankovič J., Kadlečíková M. & Breza J. 2007: Clinopyroxene exsolutions preserved in orthopyroxene from metaultramafic rock near Sedlice (Western Carpathians) and their identification by Raman Spectroscopy. [Zachovalé exsolúcie klinopyroxénu v orthopyroxéne z metaultramafickej horniny pri Sedliciach (Západné Karpaty) a ich identifikácia ramanovou spektroskopiou.] *Acta Geol. Univ. Comen.* 1, 55–59 (in Slovak).

Tamura A. & Arai S. 2006: Harzburgite- dunite-orthopyroxenite suite as a record of supra-subduction zone setting for the Oman ophiolite mantle. *Lithos* 90, 43–56.

Whitney D.L. & Evans B.W. 2010: Abbreviations for names of rock-forming minerals. *Amer. Mineralogist* 95, 185–187.

http://www.geology.sk/